Structure of Amorphous $(Co, Mn)_{76}B_{24}$- and $(Co, Mn)_{85}B_{15}$-Alloys by Means of X-Ray- and Neutron-Diffraction

M. Heckele, P. Lamparter, and S. Steeb

Max-Planck-Institut für Metallforschung, Institut für Werkstoffwissenschaft, Stuttgart

R. Bellissent

Laboratoire Léon Brillouin, Laboratoire Commun CEA-CNRS, 91191 Gif-sur-Yvette Cedex, France

Z. Naturforsch. **44a**, 495–503 (1989); received March 18, 1989

Amorphous $(Co_{1-x}Mn_x)_{85}B_{15}$- ($x=0.07$; 0.22; 0.39) and $(Co_{1-x}Mn_x)_{76}B_{24}$- ($x=0$; 0.07; 0.22) alloys were produced by melt-spinning and investigated by X-ray- and neutron-diffraction. The variation of x, i.e. the manganese concentration did not influence the X-ray intensity pattern, which suggests that no larger topological changes in the structure took place. However, using neutrons, the variation of x caused large intensity variations. These lead for large x to negative values in the total pair distribution functions $g(R)$. From this behaviour it is concluded that cobalt and manganese cannot be mutually substituted but form a chemical short range order with preference for Co–Mn-pairs compared to Mn–Mn- and Co–Co-pairs. The metal-boron-correlations are preferentially cobalt-boron-correlations. The evaluation of measured data yielded no direct boron-boron-contacts.

1. Introduction

The structure of amorphous $Fe_{80}B_{20}$- [1–3] and $Ni_{81}B_{19}$- [4, 5] alloys was investigated extensively in terms of partial correlation functions, whereas for amorphous $Co_{80}B_{20}$ [2] only little information exists. Therefore we intended to apply the method of isomorphous substitution to $(Co, Mn)_{85}B_{15}$ and $(Co, Mn)_{76}B_{24}$ in order to evaluate the partial structure factors for both alloys. The application of the method of isomorphous substitution of Co by Mn seemed to be favourable regarding the chemical similarity of both elements, the Co–Mn phase diagram, the atomic diameters, and the very different neutron scattering lengths with opposite signs. Nevertheless, during the present work it turned out that substitution of Co by Mn in (Co, Mn)–B-alloys is not isomorphous.

2. Theoretical

2.1. Total and Partial Structure Factors and Pair Correlation Functions

Concerning the definitions of total structure factors $S(Q)$, with $Q=4\pi(\sin\Theta)/\lambda=$ modulus of the scattering vector, $2\Theta=$ scattering angle, and $\lambda=$ wavelength of the radiation, we refer to [6]. In that reference also the definitions of total pair correlation functions $G(R)$ and total pair distribution functions $g(R)$, with $R=$ atomic distance in real space, are given together with the mathematical formalism according to which these functions follow from $S(Q)$.

Reprint requests to Prof. Dr. S. Steeb, Max-Planck-Institut für Metallforschung, Institut für Werkstoffwissenschaften, Seestrasse 92, D-7000 Stuttgart 1.

2.2. Isomorphous Substitution

If the variation of the concentrations of the components of an alloy does not involve changes in the corresponding structure, the method of isomorphous substitution is applicable. This allows to produce structurally identical specimens with different scattering lengths which thus yield different contrast in diffraction experiments. If, for example, in the ternary alloy $Co_{c_{Co}}Mn_{c_{Mn}}B_{c_B}$ the components Co and Mn can be mutually substituted, they can be replaced in the formalism of equations by the fictive metallic component ${}^xM$ with

$$x=\frac{c_{Mn}}{c_{Co}+c_{Mn}}=\frac{c_{Mn}}{c_M},\quad c_i=\text{atomic fractions.} \tag{1}$$

Thus the ternary alloy can be treated as binary alloy ${}^xM_{c_M}B_{c_B}$ as will be shown by means of the distribution functions in the following. For a ternary system the total distribution function $g_{tot}^{FZ}(R)$ according to Faber

0932-0784 / 89 / 0600-0495 $ 01.30/0. – Please order a reprint rather than making your own copy.

and Ziman [7] can be presented as sum of six weighted partial distribution functions:

$$g_{\text{tot}}^{\text{FZ}}(R) = \frac{1}{\langle b\rangle^2}\,[c_{\text{Co}}^2\, b_{\text{Co}}^2\, g_{\text{CoCo}}(R) + 2\,c_{\text{Co}}\, c_{\text{Mn}}\, b_{\text{Co}}\, b_{\text{Mn}}\, g_{\text{CoMn}}(R) + c_{\text{Mn}}^2\, b_{\text{Mn}}^2\, g_{\text{MnMn}}(R) + 2\,c_{\text{Co}}\, c_{\text{B}}\, b_{\text{Co}}\, b_{\text{B}}\, g_{\text{BCo}}(R) + 2\,c_{\text{Mn}}\, c_{\text{B}}\, b_{\text{Mn}}\, b_{\text{B}}\, g_{\text{BMn}}(R) + c_{\text{B}}^2\, b_{\text{B}}^2\, g_{\text{BB}}(R)] \quad (2)$$

with b = scattering length and

$$\langle b\rangle = c_{\text{Co}}\, b_{\text{Co}} + c_{\text{Mn}}\, b_{\text{Mn}} + c_{\text{B}}\, b_{\text{B}}\,. \quad (3)$$

Isomorphous substitution between Co and Mn implies the identities

$$g_{\text{CoCo}}(R) = g_{\text{CoMn}}(R) = g_{\text{MnMn}}(R) = g_{\text{MM}}(R), \quad (4)$$

$$g_{\text{BCo}}(R) = g_{\text{BMn}}(R) = g_{\text{BM}}(R). \quad (5)$$

Together with the scattering length

$$b_{\text{M}} = \left(\frac{c_{\text{Co}}}{c_{\text{M}}}\, b_{\text{Co}} + \frac{c_{\text{Mn}}}{c_{\text{M}}}\, b_{\text{Mn}}\right) = (1-x)\, b_{\text{Co}} + x\, b_{\text{Mn}} \quad (6)$$

we obtain from (2), (4), (5) for the case of isomorphous substitution of Co and Mn:

$$g_{\text{tot}}^{\text{FZ}}(R) = W_{\text{MM}}\, g_{\text{MM}}(R) + W_{\text{BM}}\, g_{\text{BM}}(R) + W_{\text{BB}}\, g_{\text{BB}}(R) \quad (7)$$

with

$$W_{\text{MM}} = c_{\text{M}}^2\, b_{\text{M}}^2/\langle b\rangle^2 \quad (8)$$

$$W_{\text{BM}} = 2\,c_{\text{B}}\, c_{\text{M}}\, b_{\text{B}}\, b_{\text{M}}/\langle b\rangle^2, \quad (9)$$

$$W_{\text{BB}} = c_{\text{B}}^2\, b_{\text{B}}^2/\langle b\rangle^2. \quad (10)$$

2.3. Short Range Order Parameters

In the case of isomorphous substitution the distribution of Co- and Mn-atoms on the metal-sites is statistical. However, as usual [1, 4] in metal-metalloid-glasses the distribution of the metal- and boron-atoms is not statistical. This question normally is treated using the Cargill-Spaepen short range order parameter, which is defined for systems with different atomic sizes [8].

In the following we define two short range order parameters α and α' which in a quantitative way describe the deviation of the arrangement of Co- and Mn-atoms on the M-sites from statistical distribution.

2.3.1 Short Range Order Between Mn- and Co-Atoms

Using the concept of the Warren-Cowley short range order parameter α [9] we define

$$\alpha = 1 - \frac{Z_{\text{CoMn}}}{x\, Z_{\text{MM}}} = 1 - \frac{Z_{\text{MnCo}}}{(1-x)\, Z_{\text{MM}}} \quad (11)$$

with

Z_{MM} = number of M-atoms around a M-atom,
Z_{CoMn} = number of Mn-atoms around a Co-atom,
Z_{MnCo} = number of Co-atoms around a Mn-atom.

Statistical distribution of Co and Mn on the metal-sites implies

$$Z_{\text{CoMn}} = x\, Z_{\text{MM}}\,, \quad (12\text{a})$$

$$Z_{\text{MnCo}} = (1-x)\, Z_{\text{MM}}\,. \quad (12\text{b})$$

For statistical distribution α becomes zero. For segregation, i.e. preference of like metallic neighbours, α becomes positive ($0 < \alpha \leqq 1$), and for short range order in the sense of preferred Mn–Co-heterocoordination α becomes negative ($-x/(1-x) \leqq \alpha < 0$).

Regarding the metal-metal coordination numbers

$$Z_{\text{CoCo}} + Z_{\text{CoMn}} = Z_{\text{CoM}}\,, \quad (13)$$

$$Z_{\text{MnMn}} + Z_{\text{MnCo}} = Z_{\text{MnM}} \quad (14)$$

we distinguish between two degrees of deviation from statistical distribution (both possible for $\alpha < 0$ and $\alpha > 0$):

a) The metal-metal coordination is the same for either a central Co-atom or a central Mn-atom, i.e.

$$Z_{\text{CoM}} = Z_{\text{MnM}} = Z_{\text{MM}}\,. \quad (15)$$

This has been assumed already in the definition of α in (11). Note that the validity of (15) does not mean statistical distribution of the Co- and Mn-atoms on the M-sites.

For case a), Z_{MM} does not depend on the ratio x and therefore it will not be possible to detect any deviation from isomorphous substitution behaviour by X-ray diffraction because of the almost equal scattering factors of Co and Mn. Thus non-statistical distribution of Co and Mn on the metal-sites will not affect the X-ray diffraction result.

b) $Z_{\text{CoM}} \neq Z_{\text{MnM}}$.

In this case, Z_{MM} as used in (11) has the meaning of an average value over the Co- and Mn-central atoms, respectively. Then Z_{MM} will depend on the ratio x and X-ray diffraction will be sensitive to this type of deviation from substitution.

2.3.2 Short Range Order Between a Central B-Atom and its M-Surrounding

A second short range order parameter α' is defined for the M-surrounding of a central B-atom:

$$\alpha' = 1 - Z_{BMn}/x\, Z_{BM} \tag{16}$$

with

$$Z_{BCo} + Z_{BMn} = Z_{BM}\,.$$

For statistical distribution of Co and Mn on the M-sites around B stands

$$Z_{BCo} = (1-x)\, Z_{BM}\,, \tag{17}$$

$$Z_{BMn} = x\, Z_{BM}\,. \tag{18}$$

Negative values of α' mean a preference of Mn-atoms compared to Co-atoms around the central B-atom.

Again we have to keep in mind that deviation from statistical distribution might involve a dependence of the number of M-neighbours around B, i.e. Z_{BM}, on the ratio x.

3. Experiments and Results

Table 1 contains the neutron-scattering and -absorption data used in this work, and the atomic radii for Co, Mn, and B.

The concentrations of the ternary (Co, Mn)–B-alloys studied in the present paper lie in the region of glass formation as given by [12–15].

3.1. Sample Preparation

Manganese platelets (purity 99.97%), pieces of cobalt (purity 99.9%), and boron powder (purity 99.7%, isotopic enrichment 97.2% ^{11}B) were melted together in an induction furnace using Al_2O_3-crucibles under protection atmosphere (200 Torr Ar) and after a certain time cast into a copper mold. The production of amorphous ribbons was done by melt-spinning in vacuum. The composition of the specimen was analyzed chemically [16].

Table 1. Neutron-scattering and -absorption data and atomic radii. σ_a = absorption cross section for $\lambda = 1.8$ Å; b = coherent scattering length; σ_s = total scattering.

Element	σ_a [barn]	b [10^{-12} cm]	σ_s [barn]	Atomic radius [Å]
^{11}B	25.44 [1]	0.6 [1]	5.12 [1]	0.85 [4]
Mn	13.3 [11]	−0.373 [11]	2.1 [11]	1.37 [10]
Co	37.18 [11]	0.253 [11]	6.15 [11]	1.25 [10]

3.2. X-Ray Diffraction

The corrections of the X-ray data measured with a goniometer (type D 500, Siemens) using Mo-Kα radiation were done [16] according to [17]. The X-ray data of the present paper are used to check for variations in the topological arrangement of the M-atoms upon variation of the Mn-concentration x. Since the scattering lengths of both species are nearly identical, the intensity curves obtained with different mixing ratios should be the same if during the substition the topological arrangement remains unchanged. Figure 1 shows the pair correlation functions $G^{AL}(R)$ defined according to Ashcroft and Langreth [18] for the alloys $^{x}M_{85}B_{15}$ ($x = 0.07$; 0.22; 0.39). All curves are in principle identical with the only exception that with increasing Mn-concentration, i.e. with increasing ratio x, the distances become larger. This is in agreement with Table 1 according to which the atomic radius of an Mn-atom (1.37 Å) is larger than that of a Co-atom (1.25 Å). From this observation we conclude that, besides this size effect, substitution of Co by Mn does not affect the overall topological structure and that apparently (15) is fulfilled. However, as pointed out above, X-rays do not provide a probe to check (12a, b), i.e., the statistical distribution of Co and Mn on the M-sites.

3.3. Neutron Diffractiuon

The reduction of the data measured with the goniometer 7C2 (CEN, Saclay) using a wavelength of 0.71 Å was done according to the methods already described in [19–25] (for details see [16]).

In the following we describe the correction procedure for the magnetic scattering contribution. This correction was necessary since having performed all correction- and normalization-steps, the thus obtained structure factors show a rather strong increase towards low Q-values as can be seen in Fig. 2 (solid line). The fact that the structure factor oscillates around unity for $Q > 8$ Å^{-1} reflects, together with the shape of the magnetic cross section, the existence of magnetic disorder scattering. For this purpose we present in Fig. 2 (dash-dotted line) the magnetic cross section as calculated for Co^{2+} according to [26].

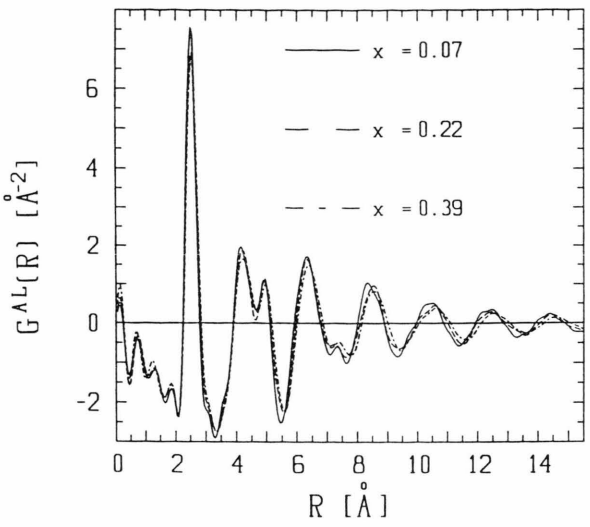

Fig. 1. Amorphous $^{x}M_{85}B_{15}$. X-ray diffraction (Mo–Kα). Pair correlation functions $G^{AL}(R)$.

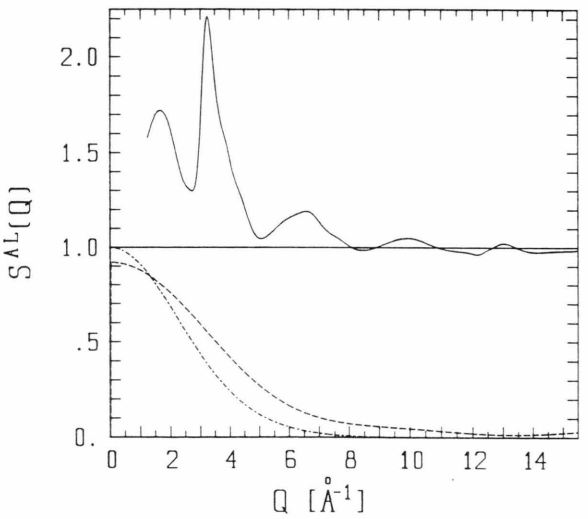

Fig. 2. Amorphous $^{0.22}M_{85}B_{15}$. $S^{AL}(Q)$ before correction for magnetic scattering (——); correction curve, see text (– – –); magnetic scattering of Co^{2+} [26] (– · – · –).

Due to the lack of sufficient information on magnetic properties it is not possible to perform the magnetic correction in an analytical way. Instead we did a Fourier inversion of the structure factor of Fig. 2, which yielded a pair correlation function $G(R)$ without anomaly except a strong maximum at a distance R smaller than the atomic radius of the metal atoms. This maximum can be taken as the Fourier inversion of the deviation of $S(Q)$ in Fig. 2 from the ideal structure factor [27]. Thus the back-transformation of this isolated maximum of $G(R)$ at small R yields the effective magnetic disorder scattering cross section as an empirical correction curve in Fig. 2 (dashed line).

Comparison of this empirical correction curve with the shape of the magnetic cross section shows this procedure to yield a reasonable result.

In connection with the magnetic scattering two comments should be given: First, the disorder scattering, as described above, was evaluated empirically in such a way that reasonable $S(Q)$- and $G(R)$-functions resulted, without treating the origin of this scattering more closely. Secondly, due to the ferromagnetic behaviour of the (Co, Mn)–B-alloys, the results after the correction still contain the coherent magnetic scattering contribution which is associated with the ordered magnetic moments of Co and Mn, and which thus contributes to the nuclear coherent scattering lengths of Co and Mn given in Table 1. This contribution to the nuclear coherent scattering, however, is not known quantitatively because of the unknown ordered magnetic moments of Co and Mn in these alloys.

3.4. Structure Factors

Figures 3 and 4 show for the amorphous $^{x}M_{85}B_{15}$- and $^{x}M_{76}B_{24}$-alloys the structure factors as obtained according to the Ashcroft and Langreth definition [18]. Apparently there are drastic changes of $S^{AL}(Q)$ with increasing Mn-content. Increasing Mn-concentration leads to a decrease of the main maximum and an increase of the prepeak at 2 Å^{-1}. Finally the main maximum vanishes totally whereas the prepeak becomes larger than one. Table 2 contains the positions of the different peaks.

Table 2. Amorphous (Co, Mn)–B-alloys. Peak positions in $S^{AL}(Q)$.

Sample	Position		
	Prepeak		Main maximum
	[Å^{-1}]	[Å^{-1}]	[Å^{-1}]
$^{0.07}M_{85}B_{15}$	1.9	–	3.2
$^{0.22}M_{85}B_{15}$	1.7	–	3.3
$^{0.39}M_{85}B_{15}$	1.7	2.6	–
$^{0.00}M_{76}B_{24}$	2.2	–	3.3
$^{0.07}M_{76}B_{24}$	2.1	–	3.3
$^{0.22}M_{76}B_{24}$	1.8	2.4	3.5

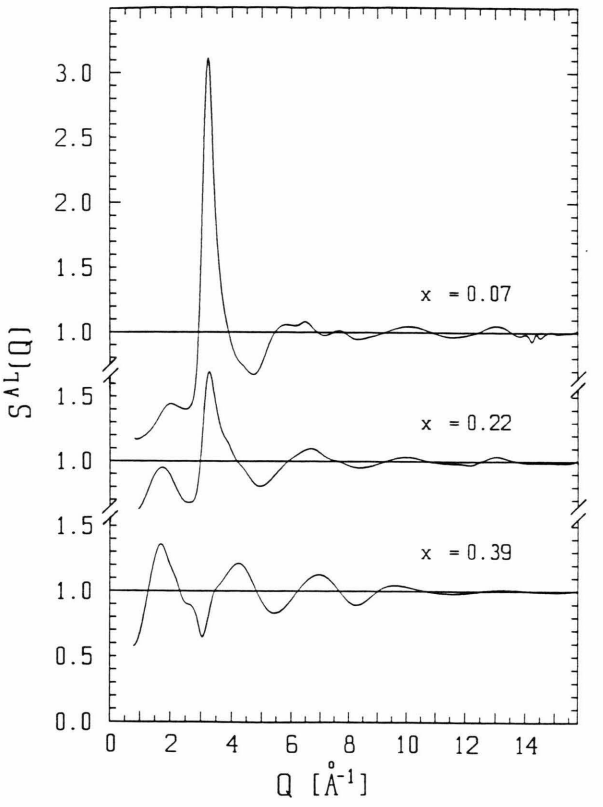

Fig. 3. Amorphous $^{x}M_{85}B_{15}$. Neutron diffraction. Structure factors $S^{AL}(Q)$.

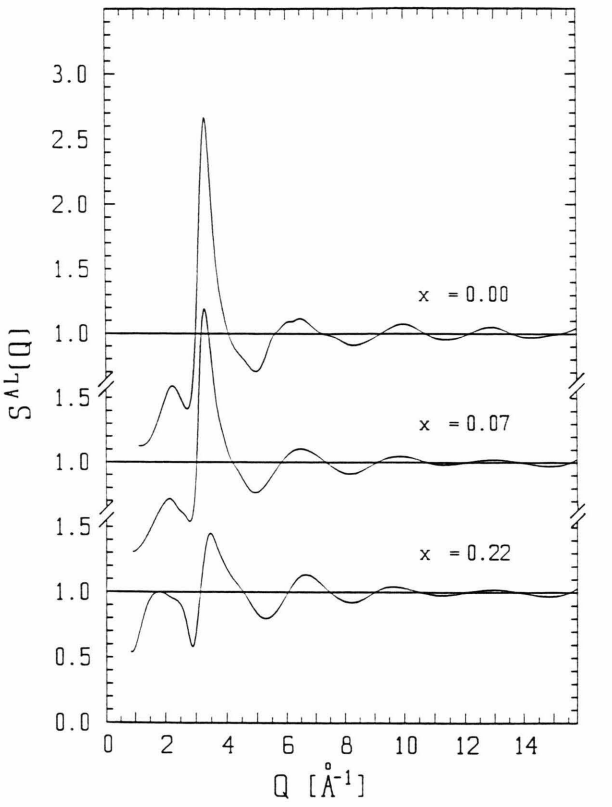

Fig. 4. Amorphous $^{x}M_{76}B_{24}$. Neutron diffraction. Structure factors $S^{AL}(Q)$.

The occurrence of a prepeak means short range ordering [28], and it is interesting that in the present case for higher Mn-concentrations a double prepeak occurs.

3.5. Pair Correlation Functions

Fourier inversion of the $S^{AL}(Q)$ in Figs. 3 and 4 yields the total pair correlation functions $G^{AL}(R)$ in Figs. 5 and 6, respectively. The ripples at smaller R-values are caused by the termination effect. The positions of the subpeaks or shoulders occurring on the main maxima, I around 2–3 Å and II around 3.5–5 Å, are compiled in Table 3.

In contrast to the X-ray curves in Fig. 1, we observe a drastic change of the neutron curves in Fig. 5 upon substituting Co by Mn, which is explained by the negative scattering length of the Mn-atoms: Increasing Mn-concentration yields decreasing oscillations at larger distances $R > 4$ Å. The shoulders around the maximum II and also the shoulder at $R_{I,3}$ develop into

Table 3. Positions of the subpeaks of the two first maxima I and II in the pair correlation function $G^{AL}(R)$ from neutron diffraction experiments. The data marked with * were taken from X-ray curves.

Specimen	Peak position [Å]						
	I			II			
	I,1	I,2	I,3	II,1	II,2	II,3	II,4
$^{0.07}M_{85}B_{15}$	2.11	2.51	2.96	3.52	3.91	4.32	4.76
$^{0.22}M_{85}B_{15}$	2.06	2.46	3.01	3.51	4.00	4.43	4.85
$^{0.39}M_{85}B_{15}$	2.01	–	2.96	3.56	–	4.41	–
$^{0.07}M_{85}B_{15}$*	–	2.50	3.00	–	4.15	–	4.90
$^{0.00}M_{76}B_{24}$	2.09	2.52	3.00	3.49	4.16	–	–
$^{0.07}M_{76}B_{24}$	2.08	2.44	2.80	3.30	3.73	4.13	–
$^{0.22}M_{76}B_{24}$	2.06	–	2.94	3.32	3.75	4.11	–
$^{0.07}M_{76}B_{24}$*	–	2.50	3.00	–	4.09	–	4.90

separate subpeaks. The main change is observed in the first double-maximum I which reflects the metal-boron nearest neighbours at $R_{I,1} \approx 2.1$ Å and the metal-metal neighbours at $R_{I,2} \approx 2.5$ Å. With increasing Mn-concentration we observe a characteristic

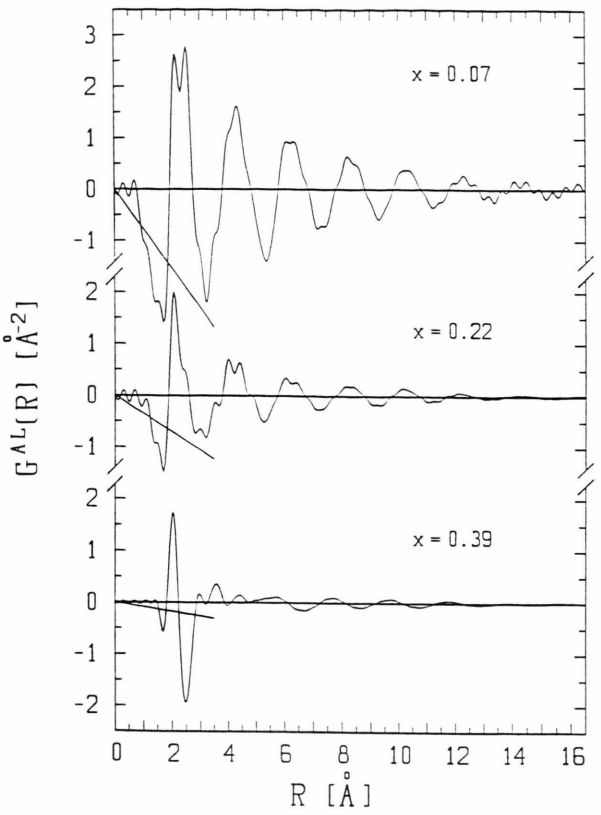

Fig. 5. Amorphous $^{x}M_{85}B_{15}$. Neutron diffraction. Pair correlation functions $G^{AL}(R)$ and $\frac{\langle b\rangle^2}{\langle b^2\rangle} 4\pi\varrho_0 R$ (=straight lines).

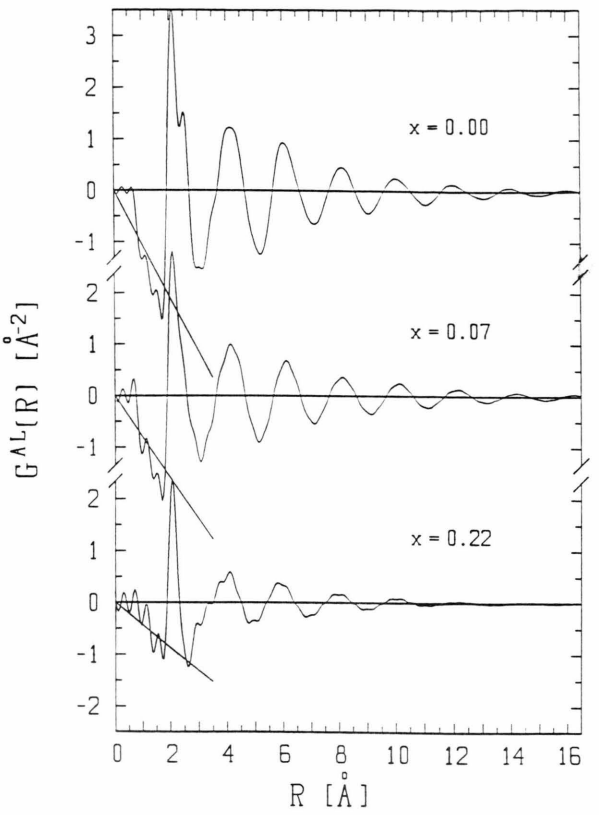

Fig. 6. Amorphous $^{x}M_{76}B_{24}$. Neutron diffraction. Pair correlation functions $G^{AL}(R)$ and $\frac{\langle b\rangle^2}{\langle b^2\rangle} 4\pi\varrho_0 R$ (=straight lines).

variation, and this will be the basis for the discussion of the substitution behaviour of Co- and Mn-atoms in the following section.

4. Discussion

4.1. Isomorphous Substitution

Figures 7 and 8 show the Faber-Ziman total pair distribution functions $g^{FZ}(R)$, which have been calculated from the $G^{AL}(R)$ in Figs. 5 and 6 according to

$$g_{tot}^{FZ}(R)=1+\frac{\langle b^2\rangle}{\langle b\rangle^2}\frac{G^{AL}(R)}{4\pi R\varrho_0}. \tag{19}$$

The weighting factors $W_{\mu\nu}$ of the three partial $g_{\mu\nu}^{FZ}(R)$, corresponding to the description as binary system with (7)–(10), are given in Table 4 together with the heights of the peaks under consideration.

Table 4. Binary M–B alloys. Weighting factors $W_{\mu\nu}$. Peak heights in the pair distribution functions $g_{tot}^{FZ}(R)$.

Specimen	Weighting-factors			Peak heights in $g_{tot}^{FZ}(R)$	
	W_{MM}	W_{BM}	W_{BB}	I,1 B–M	I,2 M–M
$^{0.07}M_{85}B_{15}$	0.44	0.45	0.11	2.6	2.4
$^{0.22}M_{85}B_{15}$	0.28	0.50	0.22	3.8	1.6
$^{0.39}M_{85}B_{15}$	0.003	0.11	0.89	1.0	−8.0
$^{0.00}M_{76}B_{24}$	0.32	0.49	0.19	2.6	1.6
$^{0.07}M_{76}B_{24}$	0.29	0.49	0.22	2.7	1.3
$^{0.22}M_{76}B_{24}$	0.13	0.47	0.40	3.8	−0.1

We note, due to the negative scattering length of Mn, a considerable variation of the $W_{\mu\nu}$ upon replacing Co by Mn. This would allow a straightforward calculation of the partial $G_{\mu\nu}(R)$ from the three total $g^{FZ}(R)$ for both compositions (15% and 24% B), if Co and Mn would substitute mutually. Especially, the alloy $^{0.39}M_{85}B_{15}$ has been chosen in such a way to

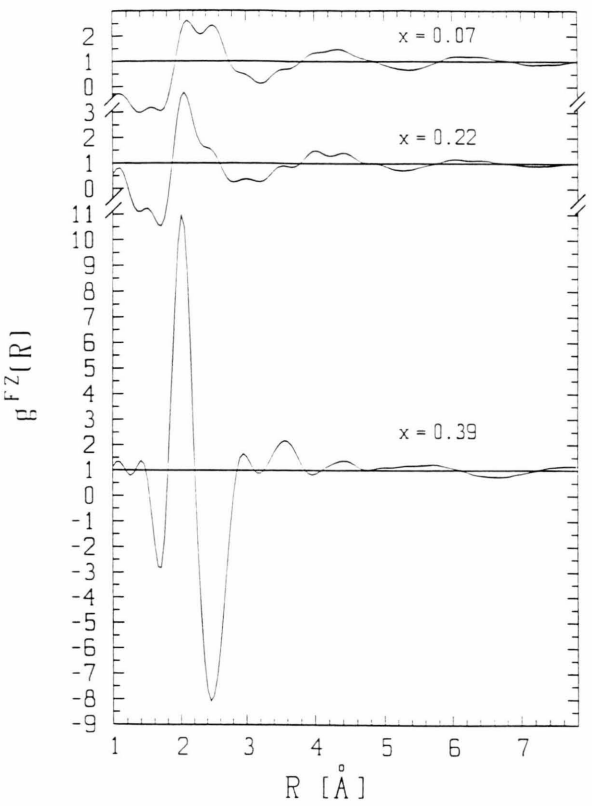

Fig. 7. Amorphous ${}^{x}M_{85}B_{15}$. Neutron diffraction. Pair distribution functions $g^{FZ}(R)$.

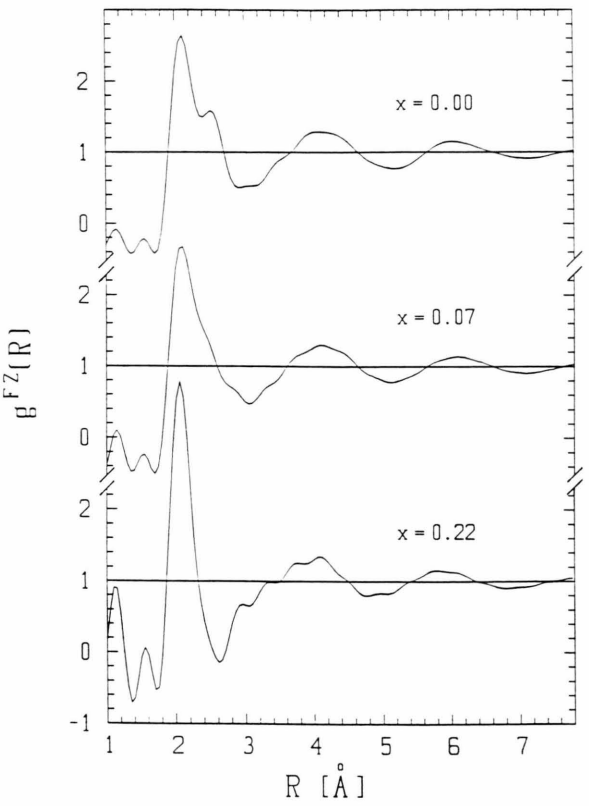

Fig. 8. Amorphous ${}^{x}M_{76}B_{24}$. Neutron diffraction. Pair distribution functions $g^{FZ}(R)$.

meet $b_M = 0$ ($x = 0.40$ in (6)) and thus to observe in that case directly the B–B correlations. However, the $g^{FZ}(R)$ obtained with this specimen most drastically shows that Co and Mn do not substitute each other isomorphously: Where we expect a vanishing contribution of the partial $g_{MM}(R)$ function, we in reality observe a strong negative M–M peak at $R_{I,2}$ in Figure 7. Negative values of $g^{FZ}(R)$ cannot be explained within the view of isomorphous substitution where all weighting factors $W_{\mu\nu}$ are positive fore both alloy systems in Table 4. Moreover, the height of the B–M peak at $R_{I,1}$ does not scale at all with W_{BM} in Table 4. Consequently, the treatment of amorphous (Co, Mn)–B as binary alloy has to be rejected, and description as ternary system in terms of six partial pair correlations has to be considered.

4.2. Discussion as Ternary System

The weighting factors of the six partial $g_{\mu\nu}(R)$ in (2) are listed in Table 5. Some correlations with Mn show negative weighting factors which allow the explanation of the negative value for the peak I,2 in the pair distribution function in Fig. 7 for the metal-metal-distance:

The Co–Mn-correlation with its negative weighting factor exceeds the Mn–Mn- as well as the Co–Co-correlations with their positive weighting factors. Thus around Mn we find preferred Co-atoms,

Table 5. Ternary (Co, Mn)–B-alloys. Weighting factors $W_{\mu\nu}$.

Specimen	Weighting factors					
	W_{CoCo}	W_{MnMn}	W_{CoMn}	W_{BCo}	W_{BMn}	W_{BB}
${}^{0.07}M_{85}B_{15}$	0.56	0.006	−0.12	0.50	−0.05	0.11
${}^{0.22}M_{85}B_{15}$	0.79	0.120	−0.62	0.83	−0.33	0.22
${}^{0.39}M_{85}B_{15}$	1.60	1.460	−3.06	2.38	−2.27	0.89
${}^{0.00}M_{76}B_{24}$	0.32	0.000	0.00	0.49	0.00	0.19
${}^{0.07}M_{76}B_{24}$	0.36	0.005	−0.08	0.56	−0.07	0.22
${}^{0.22}M_{76}B_{24}$	0.41	0.070	−0.35	0.81	−0.34	0.40

and vice versa. This behaviour in (Co, Mn)–B only can be revealed using the neutron diffraction method, where $b_{Mn} < 0$, whereas X-rays merely probe the overall metal-metal correlations. Furthermore it is interesting that this Co–Mn short range order seems to be unique compared to the results reported for amorphous Fe, Mn, P, C- [29] and Fe, Mn, Y-alloys [30]. We attribute the prepeak at 2.4 to 2.6 $Å^{-1}$ from Table 2 to the Co–Mn short range order.

The second interesting feature of the $g^{FZ}(R)$ functions to be discussed are the metal-boron correlations showing up in the peak I,1. The observation that the height of this peak (Table 4) roughly scales with W_{BCo} (Table 5) gives evidence that this peak is governed by Co–B correlations, whereas Mn–B nearest neighbours play a minor role. Note that otherwise addition of Mn would cause a decrease of this peak ($W_{BMn} < 0$), which is not observed in Figs. 7 and 8.

In Fig. 7 ($x = 0.39$) we observe that the strong oscillations due to the Co–B and the Co–Mn short range ordering in the first neighbour shell are rapidly damped above $R = 2.9$ Å. This reflects that the short range order in the sense of the non-statistical distribution of Co and Mn on the metallic sites is restricted very much to nearest neighbours.

In the following the peaks II,1 and II,3 will be considered. M–M correlations can be excluded here because they are not observed with X-rays (see Table 3). Although M–B correlations can not be excluded here, we suggest these peaks to reflect B–B distances: The ratio $R_{II,3}:R_{II,1}$ is 0.81 for both boron-concentrations. This value also is found for amorphous $Ni_{81}B_{19}$ [4], where the B–B partial correlation function could be determined. Furthermore, the partial coordination numbers calculated for the two peaks discussed here result as $Z_{BB} = 3.1$ and 4.3 (see Table 6 in the following chapter). These values agree quite well with the corresponding ones in [4], keeping in mind the experimental uncertainties. We note in Table 3 that the distances $R_{II,1}$ and $R_{II,3}$ are larger in the alloys with higher metal content. Within the view of B–B distances this means that adding more metal to the alloy forces the B-atoms to be more apart from each other. We attribute the prepeak at $Q = 2$ $Å^{-1}$ (compare Table 2) to the B–B correlation.

4.3. Coordination Numbers

Since apparently Co- and Mn-atoms do not substitute in (Co, Mn)–B-alloys, three partial pair distribution functions, describing the system as binary system, cannot be evaluated. Therefore, in determining partial coordination numbers we are restricted to the total pair distribution functions. The distribution functions $g^{FZ}(R)$ were fitted by Gaussian functions $g_{\mu\nu}(R)$ adjusted to the subpeaks. The partial coordination numbers then were calculated from

$$Z_{\mu\nu} = \frac{c_\nu}{W_{\mu\nu}} F_{\mu\nu}, \tag{20}$$

where $F_{\mu\nu}$ is the area under the peak of the function:

$$RDF_{\mu\nu}(R) = 4\pi R^2 \varrho_0 g_{\mu\nu}(R). \tag{21}$$

Using this method it was possible to determine for amorphous $^{0.00}M_{76}B_{24}$ from neutron scattering Z_{CoB} and Z_{CoCo}, for amorphous $^{0.39}M_{85}B_{15}$ from neutron scattering Z_{BB}, and from X-ray scattering Z_{MM}.

Table 6 shows coordination numbers of the present work together with data for amorphous Fe–B and Ni–B.

Table 6. Atomic distances and coordination numbers. * From X-ray diffraction.

Specimen	Atomic distances			Partial coordination numbers			References
	R_{MM}	R_{MB}	R_{BB}	Z_{MM}	Z_{BM}	Z_{BB}	
$^{0.00}M_{76}B_{24}$	2.52	2.09	–	13.3	7.7	–	present
	2.50	–	–	12.6 *	–	–	paper
$^{0.39}M_{85}B_{15}$	–	–	3.56	–	–	3.1	present
	–	–	4.41	12.1 *	–	4.3	paper
$Co_{81.5}B_{18.5}$	2.50	2.07	–	12.7	6.6	–	[2]
$^{57}Fe_{80}B_{20}$	2.55	2.13	–	11.5	8.9	–	[2]
$Ni_{81}B_{19}$	2.52	2.11	3.29	10.8	9.3	3.6	[4]
	–	–	4.02	–	–	3.7	

4.4. Short Range Order Parameters

In this chapter the deviation from isomorphous substitution behaviour of (Co, Mn)–B alloys will be described quantitatively in terms of the two short range order parameters α and α' as defined in (11) and (16). Note that according to the X-ray results, the deviation from statistical distribution of the Co- and the Mn-atoms corresponds to the case a) as described in Section 3.1.

The subpeaks I,2 in Figs. 7 and 8, which represent the metal-metal correlations, were fitted by a Gaussian yielding the area F_{MM}.

F_{MM} is the sum of the weighted partial coordination numbers according to

$$F_{MM} = \frac{W_{CoCo}}{c_{Co}} Z_{CoCo} + \frac{W_{MnMn}}{c_{Mn}} Z_{MnMn} + \frac{W_{CoMn}}{c_{Mn}} Z_{CoMn}. \tag{22}$$

From (11), (13), (14), (15), and (22), using Z_{MM} from Table 6, α-values were calculated and listed in Table 7 together with the minimum possible value $\alpha_{min} = -x/(1-x)$.

Correspondingly the subpeaks I,1 in Figs. 7 and 8 representing the metal-boron correlations, yielded the area F_{BM} which is expressed by

$$F_{BM} = \frac{W_{BCo}}{c_{Co}} Z_{BCo} + \frac{W_{BMn}}{c_{Mn}} Z_{BMn}. \tag{23}$$

Table 7. Short range order parameters α and α'.

	Co–Mn		B–(Co, Mn)
	α	α_{min}	α'
$^{0.07}M_{85}B_{15}$	0.16	−0.08	0.82
$^{0.22}M_{85}B_{15}$	−0.02	−0.28	0.41
$^{0.39}M_{85}B_{15}$	−0.36	−0.64	0.40
$^{0.07}M_{76}B_{24}$	−0.03	−0.28	0.25
$^{0.22}M_{76}B_{24}$	−0.10	−0.64	0.23

From (16) and (23) together with $Z_{BCo} + Z_{BMn} = Z_{BM}$ and Z_{BM} from Table 6, α' was calculated and listed in Table 7. Hereby the assumption has been made that Z_{BM} does not depend on the ratio x.

With increasing Mn concentration α becomes smaller, which means increasing Co–Mn heterocoordination.

The positive values of α' show that nearest Co–B-pairs are preferred compared to nearest Mn–B-pairs, see (16). $\alpha' = 1$ would mean that all atoms surrounding a B-atom are Co-atoms. With increasing Mn-concentration Mn-nearest neighbours of boron become more likely. The same stands for increasing B-concentration.

[1] E. Nold, P. Lamparter, H. Olbrich, G. Rainer-Harbach, and S. Steeb, Z. Naturforsch. **36a,** 1032 (1981).
[2] P. Lamparter, E. Nold, G. Rainer-Harbach, E. Grallath, and S. Steeb, Z. Naturforsch. **36a,** 165 (1981).
[3] Y. Waseda and H. S. Chen, Phys. stat. sol. (a) **49,** 387 (1978).
[4] P. Lamparter, W. Sperl, S. Steeb, and J. Blétry, Z. Naturforsch. **37a,** 1223 (1982).
[5] J. Sietsma and B. J. Thijsse, J. Phys. F: Met. Phys. **17,** 1 (1987).
[6] S. Steeb, S. Falch, and P. Lamparter, Z. Metallkde **75,** 599 (1984).
[7] T. E. Faber and J. M. Ziman, Phil. Mag. **11,** 153 (1965).
[8] G. S. Cargill and F. Spaepen, J. Non Cryst. Sol. **43,** 91 (1981).
[9] J. M. Cowley, J. Appl. Phys. **21,** 24 (1950).
[10] C. J. Smithells, Metals Reference Book, Butterworths, London and Boston 1976, p. 100.
[11] L. Koester and W. B. Yelon, Neutron Diffraction Newsletter (1983).
[12] J. Kanehira, S. Ohnuma, K. Shirakawa, and T. Masumoto, Conference: Rapidly Quenched Metals V, Würzburg **1,** 1019 (1985).
[13] Y. Obi, H. Morita, and H. Fujimori, Sci. Rep. Res. Inst., Tohoku Univ. **A 31,** 36 (1983).
[14] Y. Obi, D. G. Onn, H. Morita, and H. Fujimori, Conference: Rapidly Quenched Metals V, Würzburg **1,** 1079 (1985).
[15] H. Yoshida, T. Kaneko, K. Shirakawa, and T. Masumoto, Sci. Rep. Res. Inst., Tohoku Univ. **A 33,** 36 (1986).
[16] M. Heckele, Diploma thesis, Universität Stuttgart, 1988.
[17] E. Bühler, Doctor thesis, Universität Stuttgart, 1986, pp. 36–44.
[18] N. W. Ashcroft and D. C. Langreth, Phys. Rev. **159,** 500 (1967).
[19] P. Convert, Thèse, Université de Grenoble, 1975, p. 146.
[20] H. H. Paalman and C. J. Pings, J. Appl. Phys. **33,** 2635 (1962).
[21] G. Placzek, Phys. Rev. **86,** 377 (1952).
[22] J. L. Yarnell, M. J. Katz, R. G. Wenzel, and S. H. Koenig, Phys. Rev. **A 7,** 2130 (1973).
[23] H. Bertagnolli, P. Chieux, and M. D. Zeidler, Molec. Phys. **32,** 759 (1976).
[24] J. Krogh-Moe, Acta Cryst. **9,** 951 (1956).
[25] V. F. Sears, Adv. Phys. 24, 1 (1975).
[26] E. J. Lisher and J. B. Forsyth, Acta Cryst. **A 27,** 545 (1971).
[27] R. Utz, Diploma thesis, Universität Stuttgart, 1986, p. 35.
[28] A. Boos, P. Lamparter, and S. Steeb, Z. Naturforsch. **32a,** 1222 (1977).
[29] C. Janot, B. George, C. Tête, A. Chamberod, and J. Laugier, J. Physique **46,** 1233 (1985).
[30] M. Maret, A. Pasturel, and P. Chieux, J. Phys. F.: Met. Phys. **17,** 2191 (1987).